High Torque-Density Seven-Phase Induction Motor Drives for Electric Vehicle Applications

D. Casadei, M. Mengoni, A. Tani, G. Serra, L. Zarri
University of Bologna
luca.zarri@mail.ing.unibo.it

Abstract- **A control scheme for a high torque-density seven-phase induction motor is presented. This scheme integrates within a coherent solution some of the features that are commonly required to a modern electric vehicle drive, such as the capability to exploit the maximum torque in the whole speed range, a weak dependence on the motor parameters, a good robustness against the variations of the dc-link voltage and, whenever possible, the minimum Joule losses. The performance of the control scheme is verified by experimental tests.**

I. INTRODUCTION

Electric vehicles (EVs) are seen as a possible step toward the solution of the pollution problem in urban environment. With the growing interest in EVs, much effort is demanded for the development of efficient, reliable and economical ac drives. Both induction motor (IM) drives and permanent magnet brushless motor drives have been applied to EVs.

Induction motors have generally lower efficiency and power density than synchronous motors but they can offer higher reliability, overload capacity, maximum speeds and - last but not least - a reasonable cost [1].

In this paper, the use of multiphase induction motors, i.e. induction motors with a number of phases greater than three, is proposed for electric vehicle applications. Nowadays, there is an increasing interest towards multi-phase motor drives, especially for medium and high power applications such as naval and railway propulsion systems. The use of multi-phase inverters together with multi-phase ac machines has been recognized as a viable approach to obtain high power ratings without increasing the stator current per phase, making it possible to use standard power switches based on a single device. The possibility to reduce the rating of the inverter switches is advantageous also for heavy electric vehicles such as buses, trucks, industrial lift trucks and light rail transit.

Furthermore, multiphase motor drives have several advantages over traditional three-phase motor drives, such as reducing the amplitude and increasing the frequency of torque pulsations, and improving the reliability and fault tolerance [2]-[3].

Multiphase drives offer the opportunity to increase the torque density by adding a third spatial harmonic in the magnetic field. This feature has been exploited mainly in permanent magnet synchronous motors [4]-[6] and its development is dependent on the successful implementation of proper modulation strategies to synthesize non-sinusoidal voltages [7]-[9]. Afterwards, high-torque density control schemes were presented for five-phase induction motor drives in [10]-[11].

The control system of a multiphase motor for EV applications has to face several problems. First of all, the drive train of an EV has to deliver constant torque at low speed, whereas a torque decrease at constant power is requested at medium and high speed.

Another problem of the control system is the complete exploitation of the battery voltage, that is indispensable to improve the range of the EV or to increase the motor performance.

In addition, the dc-link voltage of EVs shows large variations as soon as fast accelerations and decelerations are requested, that can trouble the control system. During the acceleration the available voltage at the motor terminals tends to decrease because of the unavoidable voltage drop on the battery internal resistance, whereas during the braking the voltage across the dc-link capacitors can raise very quickly.

At present, the most common control methods of high performance three-phase induction motors are the conventional field-oriented vector control and direct torque control. In literature it is possible to find papers focused on the specific problems of EVs or on the optimization of general-purpose control schemes but suitable also for EVs. In the first case, the contributions are mainly about energy-saving control strategies, that can give remarkable results provided that the motor parameters are known with sufficient accuracy [12]-[13]. In the second case, the control schemes are usually aimed to achieve the maximum torque capability of the machine over the whole flux weakening region [14]-[17]. According to these flux weakening algorithms, the optimal flux value of the motor should be updated on the basis of look-up tables or explicit expressions of quantities such as the motor speed, the motor currents, the dc-link voltage and the requested torque. However, these algorithms rely on a good knowledge of several machine parameters and the drive performance in the high speed range may depend also on the correct determination of the base speed, which is function of the actual dc-link voltage and the overload capability.

Only in the last ten years some important contributions toward a robust field weakening strategy for induction motors have been presented [18]-[24]. The basic idea is that the demand of field-weakening can be derived from the voltage requested by the current/flux regulators. If this voltage is permanently greater than the available voltage, it means that

978-1-4244-8218-4/10/$26.00 ©2010 IEEE

the torque command cannot be tracked at the present flux level and the flux has to be reduced.

As far as the efficiency of the electric drive is concerned, the techniques that can be found in literature can be divided into two categories. The first category is referred to as loss-model-based approach [25]-[29]. It requires computing the losses by using the machine model and selecting the flux level that minimizes these losses. The second category is the search-based approach [30]-[32]. According to this method the flux is decreased until the electrical input power settles down to the lowest value for a given torque and speed.

The main contribution of this paper is the proposal of a complete high-torque density control scheme for a seven phase induction motor in which all these aspects are treated in a coherent and unitary way. The proposed control scheme is based on the well-known rotor field-oriented control, where the currents are the main control variables. However, the control scheme is modified i) to increase the robustness against the variations of the motor parameters, ii) to reduce the effect of the fluctuations of the dc-link and iii) to improve the overall efficiency by adjusting the flux level at low speed using a loss-model-based approach.

Experimental results demonstrate the effectiveness of the proposed scheme.

II. Control Strategy for High Torque Density

If a multiphase motor with concentrated windings, i.e. with one slot per pole per phase, is considered, it is possible to increase the torque density by adding spatial harmonic components of order greater than one to the air-gap magnetic field.

Some authors have shown that, if a third spatial harmonic is added to the air-gap magnetic field and this harmonic moves synchronously with the fundamental component, the waveform of the magnetic field in the air-gap resulting from their superposition can have a peak value that is lower than that of the fundamental component. This result is illustrated in Fig. 1. In this way it is possible to increase the amplitude of the fundamental component up to 115% without overcoming the rated peak value of the flux density, i.e. the amplitude of the flux density in case of sinusoidal distribution of magnetic field in the air-gap.

Let's suppose that the d-axes of reference frames d_1-q_1 and d_3-q_3 have the same directions of rotor flux vectors $\overline{\varphi}_{R1}$ and $\overline{\varphi}_{R3}$ respectively. Then, the maximum amplitude of the fundamental spatial component of the magnetic field happens when the following equality comes true:

$$i_{S3d} \cong \frac{1}{2} i_{S1d} \tag{1}$$

where i_{S1d} and i_{S3d} are the d-components of the multiple space vectors of the stator currents. Equation (1) is valid under the assumption that the resulting rms current value does not overcome the current limit.

If the third spatial harmonic of the air-gap magnetic field moves synchronously with the fundamental component, its

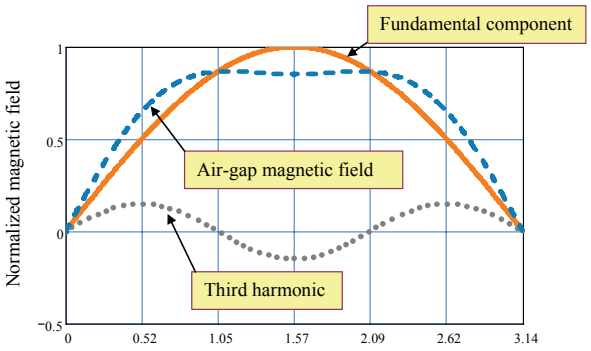

Fig. 1 - Waveform of the air-gap magnetic field: fundamental component and third spatial harmonic.

electric angular speed is triple of that of the fundamental wave, i.e.

$$\omega_3 = 3\omega_1. \tag{2}$$

If the condition of synchronism (2) is true, then the following relationship is satisfied in steady-state conditions:

$$i_{S3q} = \frac{3\tau_{R3} i_{S3d}}{\tau_{R1} i_{S1d}} i_{S1q}\,. \tag{3}$$

where i_{S1q} and i_{S3q} are the q-components of the first two multiple space vectors of the stator currents, whereas τ_{R1} and τ_{R3} are the rotor time constants.

In conclusion, (1) and (3) show that the currents i_{S3d} e i_{S3q} are roughly proportional to the currents i_{S1d} e i_{S1q} respectively.

Finally, the fifth harmonic component of the magnetic field is set to zero in this paper, since the advantages related to its use are generally lower than the increase in complexity of the control scheme.

III. Reduction of the Motor Losses

The torque delivered to the load by the motor can be written as follows:

$$T = \frac{7}{2} p \left(M_1 \bar{i}_{S1} \cdot j\bar{i}_{R1} + 3M_3 \bar{i}_{S3} \cdot j\bar{i}_{R3} \right) \tag{4}$$

where $\bar{i}_{S1}$, $\bar{i}_{R1}$, $\bar{i}_{S3}$ and $\bar{i}_{R3}$, are the multiple space vectors of the stator and rotor currents, and M_1, M_3 are the mutual inductances of the motor.

Equation (4) suggests that the motor can produce the same torque for different combinations of the stator and rotor currents and therefore it is opportune to find which values correspond to the maximum efficiency.

The Joule losses can be expressed as the sum of the contributions of the rotor and the stator currents, as follows:

$$P_{Joule} = \frac{7}{2} R_S \left(i_{S1d}^2 + i_{S1q}^2 \right) + \frac{7}{2} R_{R1} \left(i_{R1d}^2 + i_{R1q}^2 \right) + \frac{7}{2} R_S \left(i_{S3d}^2 + i_{S3q}^2 \right) + \frac{7}{2} R_{R3} \left(i_{R3d}^2 + i_{R3q}^2 \right) \tag{5}$$

where the stator resistance R_S has been assumed the same for both planes d_1-q_1 and d_3-q_3, whereas two different resistances R_{R1} and R_{R3} have been assumed for the rotor circuit.

In steady state conditions, the rotor currents i_{R1d} and i_{R3d} are both null, whereas the rotor currents i_{R1q} and i_{R3q} can be

expressed as functions of the stator currents i_{S1q} and i_{S3q}, as follows:

$$i_{R1d} = i_{R3d} = 0 \tag{6}$$

$$i_{R1q} = -\frac{M_1}{L_{R1}} i_{S1q} \tag{7}$$

$$i_{R3q} = -\frac{M_3}{L_{R3}} i_{S3q} \tag{8}$$

The minimum of (5) subject to the constraint that the torque, expressed by (4), is assigned, can be found by taking (1), (3), (6)-(8) into account and using the method of Lagrange multipliers. It is possible to verify that the minimum of (5) occurs when the ratio of i_{S1d} to i_{S1q} is equal to a precise quantity that depends on the motor parameters. The optimal value for i_{S1d} turns out to be as follows:

$$i_{S1d,opt} = K_{opt} \left| i_{S1q} \right| \tag{9}$$

where

$$K_{opt} = \sqrt{\frac{R_S \left[1 + \frac{9}{4} \left(\frac{\tau_{R3}}{\tau_{R1}} \right)^2 \right] + R_{R1} \left(\frac{M_1}{L_{R1}} \right)^2 + \frac{9}{4} R_{R3} \left(\frac{M_3}{L_{R3}} \frac{\tau_{R3}}{\tau_{R1}} \right)^2}{\frac{5}{4} R_S}} \tag{10}$$

It can be shown that the optimization strategy is not effective for high torque values. In fact the optimal selection of the stator current components is practicable only until i_{S1d} is lower than the rated value, $I_{S1d,rated}$. In other words, the motor drives benefits from the optimization strategy only for torque values lower than the following value:

$$T_{\lim} = \frac{7}{2} p \frac{M_1^2}{L_{R1}} \frac{K_T}{K_{opt}} I_{S1d,rated}^2 \tag{11}$$

where K_T is a dimensionless coefficient defined by:

$$K_T = 1 + \frac{1}{4} \frac{L_{R1}}{9 L_{R3}} \frac{\tau_{R3}}{\tau_{R1}} . \tag{12}$$

IV. Field Weakening Operation

In the high-speed range, the motor operation is limited by the available dc-link voltage, the inverter current rating, and the machine thermal rating.

A. Voltage Limits

Hereafter it is assumed that the modulation strategy of the drive is able to fully exploit the dc-link voltage E_{dc} and to generate all the admissible combinations of voltage vectors in the three d-q planes [8], [33]. Approximately, if the currents in plane d_5-q_5 are not used, the admissible voltage vectors are those inside the gray region shown in Fig. 2, defined by the following inequalities:

$$\frac{v_{1,ref}}{A_1} + \frac{v_{3,ref}}{A_3} \le E_{dc} , \tag{13}$$

$$\frac{v_{1,ref}}{A_3} + \frac{v_{3,ref}}{A_2} \le E_{dc} , \tag{14}$$

where

$$A_k = \frac{1}{2 \sin\left(k \pi / 7 \right)} . \tag{15}$$

The variables in (13)-(14) are the magnitudes of the reference voltage vectors that should be generated by the inverter.

B. Current Limits

The current limit is defined by the inverter current rating or by the machine thermal rating. This limit can be approximately described by an inequality in the following form:

$$I_{S1d}^2 + I_{S1q}^2 + I_{S3d}^2 + I_{S3q}^2 \le I_{S,\max}^2 . \tag{16}$$

It is easy to recognize that the left-hand member of (16) is proportional to the sum of the squared rms value of the stator currents and is proportional to the Joule losses of the stator windings.

C. Maximum Torque Capability in Field Weakening Operation

It is well-known that, when the rotor speed of a three-phase induction motor increases, the inverter dc-link voltage may become insufficient to inject the requested currents into the motor. To allow the motor to operate at higher speeds, it is necessary to reduce the flux level, although this choice leads inevitably to a reduction of the maximum torque that the motor can deliver to the load.

It can be shown that the operation of a high-torque density multiphase motor can be divided into four speed ranges. In the low speed range (region I), the maximum torque is enhanced up to 10% by the addition of a third-order spatial harmonic, and if the motor torque is lower than the rated one, it is possible to adjust the current i_{S1d} to improve the motor efficiency according to (9).

Region II starts when the dc-link voltage is completely exploited. In this region i_{S3d} is controlled progressively to zero and the motor looses the high-torque density capability. In fact it is convenient to use the available dc-link voltage to sustain entirely the fundamental component of the magnetic field instead of the third spatial harmonic, which gives a negligible contribution to the total torque.

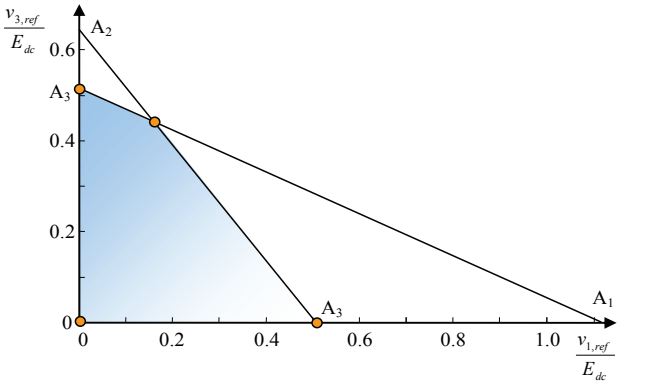

Fig. 2 - Validity domain of $v_{1,ref}$ and $v_{3,ref}$, normalized dividing by the dc-link voltage.

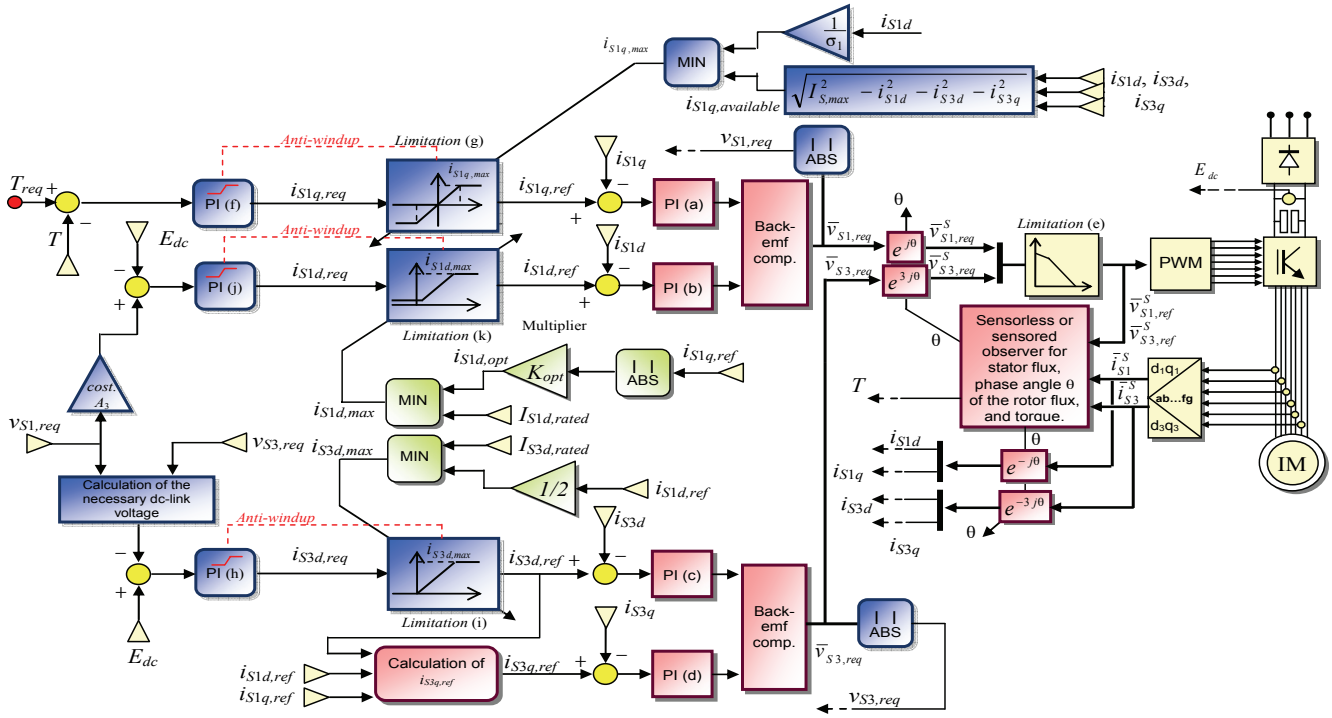

Fig. 3 - Block diagram of the control scheme.

Above the base speed (region III), the torque diminishes below the rated torque, but the power delivered to the load is practically constant and slightly greater than the power at base speed. The rms value of the phase current is constant and the voltage limit is completely exploited by v_{S1} alone.

Finally, at very high speed (region IV), the dc-link voltage is not sufficient to inject the maximum current into the motor phases. The power delivered to the load decreases and the maximum torque is obtained when the d-component of the stator flux vector is equal to the q-component, namely the stator flux vector and the rotor flux vector form an angle of 45 degrees [24].

V. Control Scheme

The block diagram of the proposed control scheme, derived on the basis of the analysis carried out in Section IV, is shown in Fig. 3. In the control scheme, it is possible to identify four different functions. The first one is responsible for the tracking of the current references, the second one is the torque control loop, the third one manages the field-weakening operation, and the fourth one is related to reduction of the power losses.

In Fig. 3, the controlled variables are expressed in two reference frames d_1-q_1 and d_3-q_3, synchronous and aligned with the corresponding rotor flux vectors.

A. Torque and Current Loop

The motor torque is adjusted by the PI regulator (f) that compares the reference torque with the estimated actual torque. The output of this regulator is the torque-producing current $i_{S1q,req}$, that tends to increase when the requested torque is greater than the estimated torque, and to decrease in the opposite case. Two PI regulators, (a) and (b), are used to track the reference signals $i_{S1d,ref}$ and $i_{S1q,ref}$. Two other PI regulators, (c) and (d), have the same task for the reference signals $i_{S3d,ref}$ and $i_{S3q,ref}$.

In region I, II, III the maximum deliverable torque is limited by the maximum current $I_{s,max}$, whereas in region IV the maximum torque takes places when the d-component of the stator flux vector is equal to the q-component of the stator flux vector. In steady-state condition, this latter equality can be written as follows:

$$i_{S1q} = \frac{i_{S1d}}{\sigma_1}. \tag{17}$$

The limitation block (g) assures that these constraints are satisfied in any speed region.

B. Flux Loop

The rotor flux magnitude φ_{R1} is indirectly controlled by PI regulator (j), which adjusts the d-component $i_{S1d,req}$ of the stator current vector. In the same way, PI regulator (h) adjusts $i_{S3d,req}$ to control the rotor flux magnitude φ_{R3}.

When the motor speed is too high, the available dc-link voltage E_{dc} is not sufficient to satisfy entirely the voltage request. The dc-link voltage that would be necessary for satisfying the voltage request is as follows:

$$E_{dc,req} = \max\left\{\frac{v_{S1,req}}{A_1} + \frac{v_{S3,req}}{A_3}, \frac{v_{S1,req}}{A_3} + \frac{v_{S3,req}}{A_2}\right\}. \tag{18}$$

When $E_{dc,req}$ is greater than the present dc-link voltage, the

TABLE I – SEVEN-PHASE MOTOR PARAMETERS

T_{rated}	=	24	Nm	L_{S1}	=	180	mH
$I_{s,max}$	=	7.5	$A_{(peak)}$	L_{R1}	=	180	mH
$I_{S1d,rated}$	=	3.6	$A_{(peak)}$	M_1	=	175	mH
f_{rated}	=	50	Hz	L_{S3}	=	24	mH
R_S	=	1.1	Ω	L_{R3}	=	24	mH
R_{R1}	=	1.0	Ω	M_3	=	19	mH
R_{R3}	=	0.8	Ω	p	=	2	

motor operates in region II, III or IV. Consequently the PI regulator (h), that integrates the difference E_{dc} - $E_{dc,req}$, reduces the third spatial harmonic of the magnetic field, and i_{S3d} is brought to zero. Otherwise it increases up to the threshold value $i_{S3d,max}$ shown in block (i).

On the other hand, if the voltage request $v_{S1,req}$ is greater than $A_3 \cdot E_{dc}$, as happens in region III and IV, the third harmonic of the magnetic field is set to zero. In this case, the PI regulator (j), which integrates a quantity proportional to the difference $E_{dc} - v_{S1,req} / A_3$, decreases φ_{R1} by acting on the current i_{S1d}.

VI. EXPERIMENTAL AND SIMULATION RESULTS

A complete drive system has been built to verify the feasibility of the proposed control scheme and some experimental tests have been carried out. The experimental set-up consists of a seven-phase IGBT inverter and a 4 kW, 7-phase, 4-pole squirrel cage induction motor, whose parameters are shown in Table I.

Figs. 4-6 show the behavior of the motor during a start-up transient when the torque reference is equal to the rated torque. Trace 4 in all Figs. 4-6 shows the waveform of a line current during the transient.

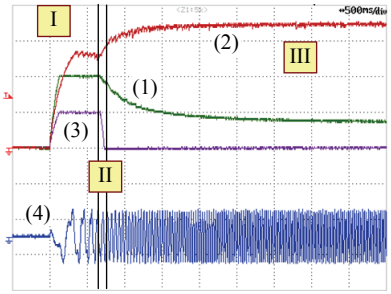

Fig. 4 - Experimental result. Start-up transient with rated torque (500 ms/div), 1) i_{S1d} (1.8 A/div), 2) i_{S1q} (2 A/div), 3) i_{S3d} (1.8 A/div), 4) Line current (10 A/div).

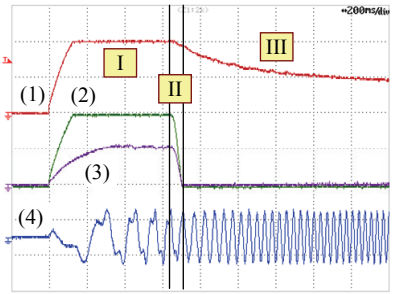

Fig. 5 - Experimental result. Start-up transient with rated torque (200 ms/div), 1) i_{S1d} (1.8 A/div), 2) i_{S3d} (0.9 A/div), 3) i_{S3q} (0.9 A/div), 4) Phase current (10 A/div).

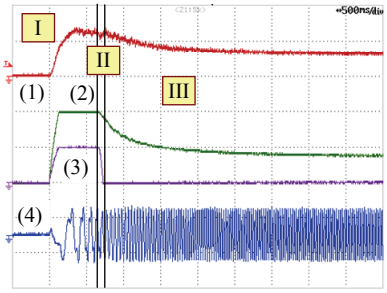

Fig. 6 - Experimental result. Start-up transient with rated torque (500 ms/div), 1) Torque (20 Nm/div), 2) i_{S1d} (1.8 A/div), 3) i_{S3d} (1.8 A/div), 4) Phase current (10 A/div).

After the rated torque command is applied, the motor starts up and the line current reaches the maximum admissible amplitude (region I). It is worth noting that, in this operating condition, the line current is distorted by the presence of the third-harmonic component of the air-gap magnetic field.

Whereas i_{S3d} is always half i_{S1d}, in region I, i_{S1d} is proportional to i_{S1q}, according to (9), as long as i_{S1d} is lower than the rated value $I_{S1d,rated}$. This behavior is clearly depicted in Fig. 4, which shows the waveforms of the currents i_{S1d}, i_{S1q}, and i_{S3d}. The behavior of i_{S3q} is shown in Fig. 5. As can be seen, i_{S3q} increases as long as i_{S1q} increases.

The torque response, which can be seen in Fig. 6, is proportional to the product $i_{S1d}\, i_{S1q}$ till the current i_{S1d} is lower than $I_{S1d,rated}$ and to the product $I_{S1d,rated}\, i_{S1q}$ otherwise.

In region II the control algorithm quickly reduces i_{S3d} and, accordingly, i_{S3q}. As a consequence, the waveform of the line current becomes practically sinusoidal.

In region III the motor flux keeps decreasing, as can be recognized by examining the waveform of i_{S1d}.

The control system increases i_{S1q} both in region II and III, to take advantage of the progressive reduction of the other current components and to entirely exploit the current limit (16).

Figs. 7-9 investigate the performance of the strategy for the optimization of the Joule losses. In these figures the range of the torque axis goes from 0 to 1.1 p.u. to consider also the improvement in the maximum torque due to the high-torque density control scheme.

As can be seen, the optimization strategy is useful only if the motor torque is approximately lower than half the rated torque, and is more effective for low torque values. It can be noted from Fig. 8 that the reduction of the power losses is mainly a consequence of the lower magnitude of the stator current that is necessary to generate the same torque values. Intuitively, this behavior is in accordance with the idea that the control system reduces the energy consumption when the motor is not requested to deliver high torque values to the load.

VII. CONCLUSION

A rotor-flux-oriented control scheme for high-torque density seven-phase induction motor drives has been presented and experimentally assessed. The proposed control

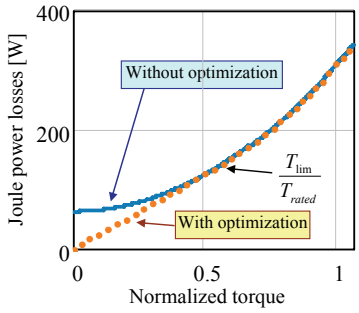

Fig. 7 - Simulation result. Behavior of the Joule power losses of the motor as a function of the electromagnetic torque, normalized by dividing by the rated torque.

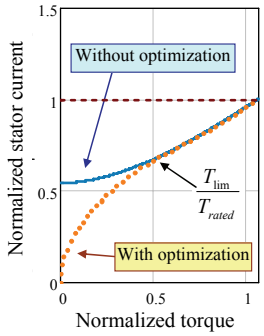

Fig. 8 - Simulation result. Magnitude of the stator current as a function of the motor torque. The currents and the torque are normalized by dividing by the maximum current and the rated torque respectively.

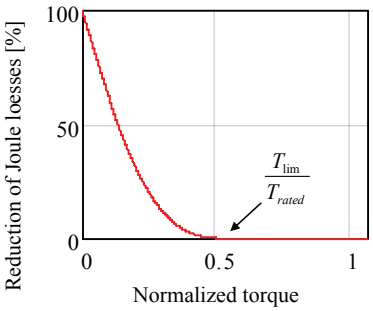

Fig. 9 - Simulation result. Reduction of the Joule power losses of the motor as a function of the electromagnetic torque, normalized by dividing by the rated torque.

scheme is able to exploit the maximum torque capability of the motor at any speed. The flux control loop is independent of the base speed and the motor parameters, except for the leakage inductance $\sigma_1 L_{S1}$. In addition, it does not require any complex calculation of the flux level or look-up tables. When low torque values are demanded to the motor, the control scheme leads also to the minimum Joule losses.

REFERENCES

[1] L. Chang, "*Comparison of AC drives for electric vehicles - A reports on Expert's opinion survey*, " IEEE AES System Magazine, August 1994, pp.7-10.

[2] L. Parsa, "On advantages of multi-phase machines," in Proc. of IEEE IECON, 2005, pp. 1574-1579.

[3] E. Levi, R. Bojoi, F. Profumo, H.A. Toliyat, S. Williamson, "*Multiphase induction motor drives – a technology status review*," IET Electr. Power Appl., vol. 1, no.4, pp. 489-516, July 2007.

[4] L. Parsa, H. A. Toliyat, "*Five-phase permanent-magnet motor drives*," IEEE Trans. on Industry Applications, Vol. 41, No. 1, Jan./Feb. 2005, pp. 30-37.

[5] L. Parsa, N. Kim and H. Toliyat, "Field Weakening Operation of a High Torque Density Five Phase Permanent Magnet Motor Drive," IEEE IEMDC, May 15-18, 2005, pp. 1507 - 1512.

[6] F. Locment, E. Semail, X. Kestelyn, "*Vectorial approach-based control of a seven-phase axial flux machine designed for fault operation*," IEEE Trans. on Industrial Electronics, Vol. 55, No. 10, Oct. 2008, pp. 3682 - 3691.

[7] H Shan Xue, Xuhui Wen, Zhao Feng, "A novel multi-dimensional SVPWM strategy of multiphase motor drives," in Proc. of EPE-PEMC 2006, Portoroz, Slovenia, pp. 931-935.

[8] A. Lega, M. Mengoni, G. Serra, A. Tani, L. Zarri, "*Space vector modulation for multiphase inverters based on a space partitioning algorithm*," IEEE Trans. on Industrial Electronics, Vol. 56, No. 10, Oct. 2009, pp. 4119-4131.

[9] S. Xue, X. Wen, Z. Feng, "Multiphase Permanent Magnet Motor Drive System Based on A Novel Multiphase SVPWM, " in Proc. of IPEMC 2006, 14-16 Aug. 2006, Vol. 1, pp. 1-5.

[10] H. Xu, H. A. Toliyat, L. J. Petersen, "Rotor field oriented control of five-phase induction motor with the combined fundamental and third harmonic currents," in Proc. of IEEE APEC, 2001, pp. 392-398.

[11] H. Xu, H.A. Toliyat, L. J. Petersen, "*Five-phase induction motor drives with DSP-based control system*," IEEE Trans. on Power Electron., Vol. 17, No. 4, 2002, pp. 524-533.

[12] N. Mutoh, S. Kaneko, T. Miyazaki, R. Masaki, S. Obara, "*A torque controller suitable for electric vehicles*, " IEEE Trans. on Industrial Electronics, vol. 44, No.1, February 1997, pp. 54-63.

[13] J. Faiz, M. B. B. Sharifian, A. Keyhani, A. B. Proca, "*Sensorless direct torque control of induction motors used in electric vehicle*, " IEEE Trans. on Energy Conversion, vol. 18, No. 1, March 2003, pp. 1-10.

[14] X. Xu, D. W. Novotny, "*Selection of the flux reference for induction machine drives in the field weakening region*," IEEE Trans. on Industry Applications, Vol. 28, no. 6, pp. 1353-1358, Nov. – Dec. 1992.

[15] S. H. Kim, S. K. Sul, "*Maximum torque control of an induction machine in the field weakening region,*" IEEE Trans. on. Industry Applications, vol.31, no. 4, pp. 787-794, Jul./Aug. 1995.

[16] D. Casadei, F. Profumo, G. Serra, A. Tani, L. Zarri, "*Performance analysis of a speed-sensorless induction motor drive based on a constant switching frequency dtc scheme*, " IEEE Trans. on Industry Applications, vol. 39, no. 2, March/April 2003, pp. 476-484.

[17] M. Ho Shin, D. S. Hyun, S. B. Cho, "*Maximum torque control of stator-flux-oriented induction machine drive in the field-weakening region*," IEEE Trans. on Industry Applications, vol. 38, no. 1, pp. 117-121, Jan./Feb. 2002.

[18] A. Biinte, H. Grotstollen, P. Krafka, "Field weakening of induction motors in a very wide region with regard to parameter uncertainties," PESC 96, vol. 1, 26-27 June 96, Baveno, Italy, pp. 944-950.

[19] S.H. Kim, S.K. Sul, "*Voltage control strategy for maximum torque operation of an induction machine in the field weakening region*," IEEE Trans. on Industrial Electronics, vol. 44, no.4, Aug. 1997, pp. 512-518.

[20] H. Abu-Rub, Member, H. Schmirgel, J. Holtz, "*Sensorless control of induction motors for maximum steady-state torque and fast dynamics at field weakening*," IAS 2006, 8-12 Oct. 2006, Tampa, Florida, Paper N.IAS03P3.

[21] L. Harnefors, K. Pietiläinen, L. Gertmar, "*Torque-maximizing field-weakening control: design, analysis, and parameter selection*," IEEE Trans. on Industrial Electronics, vol. 48, no. 1, Feb. 2001, pp. 117-122.

[22] Z. Peroutka, K. Zeman, "New field weakening strategy for AC machine drives for light traction vehicles," EPE 2007, Aalborg, Denmark, pp. 1-10.

[23] D. Casadei, G. Serra, A. Stefani, A. Tani, L. Zarri, "*DTC Drives for wide speed range applications using a robust flux-weakening algorithm*," IEEE Trans. on Industrial Electronics, Vol. 54, No. 5, Oct. 2007, pp. 2451-2461.

[24] M. Mengoni, L. Zarri, A. Tani, G. Serra, D. Casadei, "*Stator flux vector control of induction motor drive in the field weakening region,* " IEEE Trans. on Power Electronics, Vol. 23, No. 2, March 2008, pp. 941-948.

[25] H. G. Kim, S. K Sul, M. H. Park, "*Optimal efficiency drive of a current source inverter fed induction motor by flux control*", IEEE Trans. on Industry Applications, vol. IA-20, no. 6, November/December 1984, pp. 1453-1459.

[26] I. Kioskeridis and N. Margaris, "*Loss minimization in induction motor adjustable speed drives,*" IEEE Trans. Ind. Electron., vol. 43, pp. 226–231, Feb. 1996.

[27] K. Matsuse, S. Taniguchi, T. Yoshizumi, K. Namiki, "*A speed-sensorless vector control of induction motor operating at high efficiency taking core loss into account*, " IEEE Trans. on Industry Applications, vol. 37, no. 2, March/April 2001, pp. 548-558.

[28] S. Lim and K. Nam, "*Loss-minimising control scheme for induction motors*, " IEE Proc.-Electr. Power Appl., Vol. 151, No. 4, July 2004, pp. 389-397.

[29] G. Dong, O. Ojo, "*Efficiency optimizing control of induction motor using natural variables*, " IEEE Trans. on Industrial Electronics, vol. 53, no. 6, December 2006, pp. 1791-1798.

[30] D. S. Kirschen, D. W. Novotny, T. A. Lipo, "*Optimal efficiency control of an induction motor drive*, " IEEE Trans. on Energy Conversion, vol. EC-2, no. 1, March 1987, pp. 70-76.

[31] Cao-Minh Ta, Y. Hori, "*Convergence improvement of efficiency-optimization control of induction motor drives*, " IEEE Trans. on Industry Applications, vol. 37, no. 6, November/December 2001, pp. 1764-1753.

[32] C. Chakraborty, Y. Hori, "*Fast efficiency optimization techniques for the indirect vector-controlled induction motor drives*," IEEE Trans. on Industry Applications, Vol. 39, No. 4, July/August 2003, pp. 1070-1076.

[33] D. Casadei, D. Dujic, E. Levi, G. Serra, A. Tani, L. Zarri, "*General Modulation Strategy for Seven-Phase Inverters with Independent Control of Multiple Voltage Space Vectors*," IEEE Trans. on Industrial Electronics, Vol. 23, No. 2, May 2008, pp. 1921-1932.